Field-Aligned Electron Density Distribution of the Inner Magnetosphere Inferred from Coordinated Observations of Arase and Van Allen Probes

Yuki Obana[1]*, Yukinaga Miyashita[2], Naomi Maruyama[3,4], Atsuki Shinbori[5], Masahito Nosé[5], Masafumi Shoji[5], Atsushi Kumamoto[6], Fuminori Tsuchiya[7], Shoya Matsuda[8], Ayako Matsuoka[9], Yoshiya Kasahara[10], Yoshizumi Miyoshi[5], Iku Shinohara[8], William S. Kurth[11], Charles W. Smith[12], Robert J. MacDowall[13]

[1]Department of Engineering Science, Faculty of Engineering, Osaka Electro-Communication University, 18-8 Hatsucho, Neyagawa, Osaka, 572-8530, Japan.
[2] Korea Astronomy and Space Science Institute, Daejeon, South Korea.
[3]CIRES, University of Colorado Boulder, CO, 80305, USA.
[4]NOAA Space Weather Prediction Center, CO, 80305, USA.
[5]Institute for Space-Earth Environmental Research (ISEE), Nagoya University, Nagoya, Aichi, 464-8601, Japan.
[6]Department of Geophysics, Tohoku University, Aoba-ku, Sendai, Miyagi, 980-8578, Japan.
[7]Planetary Plasma and Atmospheric Research Center (PPARC), Tohoku University, Aoba-ku, Sendai, Miyagi, 980-8578, Japan.
[8]Institute of Space and Astronautical Science, Japan Aerospace Exploration Agency, 3-1-1, Yoshinodai, Chuo-ku, Sagamihara, Kanagawa, 252-5210, Japan.
[9] Data Analysis Center for Geomagnetism and Space Magnetism Graduate School of Science, Kyoto University, Kyoto, 606-8502, Japan.
[10] Graduate School of Natural Science and Technology, Kanazawa University, Kakumamachi, Kanazawa, 920-1192, Japan.
[11] Department of Physics and Astronomy, University of Iowa, Iowa City, IA, USA
[12] nstitute for the Study of Earth, Oceans, and Space, University of New Hampshire, Durham, NH, USA
[13] Solar System Exploration Division, Goddard Space Flight Center, Greenbelt, MD, USA

*Corresponding author: Yuki Obana (obana@osakac.ac.jp)

Key Points:

Using in-situ measurements of the electron density from Arase and RBSP, we

estimated the density distribution along magnetic field lines.

The power-law index of the electron density distributions was 6~8, ~0 and -2~-1 for the trough, plume and partially refilled plasmasphere, respectively.

This is the first estimation of the power-law index using the data from different spacecraft projects.

Plain Language Summary

The plasmasphere is the region filled with cold, dense ionized gas in geospace. The ionized gas mainly consists protons, helium ions, oxygen ions and electrons, which come from Earth's ionosphere and fill magnetic flux tubes. The density distribution of the ionized gas along the flux tube provides important information to understand how the ions and electrons have been supplied from the ionosphere. Many satellites fly in the equatorial plane, hence, do not provide information on the electron density along the field. The RBSP and the Arase satellites have different inclinations and sometimes they simultaneously fly near the equator and off the equator on the same magnetic field line. Using electron densities observed by these satellites during the 7 Sep 2017 storm, we successfully estimated the electron density distribution along of the field lines inside the partially refilled plasmasphere, outside of the plasmasphere and in the tail-like structure called a plume.

Abstract

The RBSP and the Arase satellites have different inclinations and sometimes they fly both near the equator and off the equator on the same magnetic field line, simultaneously. Such conjunction events give us opportunities to compare the electron density at different latitudes. In this study, we analyzed the plasma waves observed by Arase and RBSP-A or B during the three conjunction events during and after the 7 Sep 2017 storm event. The electron number density at the satellite positions were estimated from frequencies of the UHR emissions obtained by the HFA/PWE onboard the Arase and the Waves instrument onboard RBSP, respectively. During the three conjunction events, the satellites passed through the plume, inner trough (the narrow region with low electron density between main body of the plasmasphere and the plume), plasmatrough with variable electron density, and partially-refilled plasmasphere. The power-law index m for the inner trough and plume was inferred to be 6~8 and ~0, respectively. This is interpreted to mean that the trough was close to collisionless

and the plume was near diffusive equilibrium. In the plasmatrough with the varying density, both the high-density and low-density regions had m~0. The low-density portion of this region may have a different origin from the inner trough, because of the different m-indices. For the partially-refilled plasmasphere in the storm recovery phase, the power-law index m showed negative values, meaning that the density in the equatorial plane was higher than at higher latitudes.

1. Introduction

The plasmasphere is a region in the inner magnetosphere filled with cold, dense plasma from the underlying ionosphere, and the field-aligned profile of its density attracts much interest, because it reflects the physical processes of mass transport from the source region. For example, when the very simple power law model

$$n = n_{eq}\left(\frac{LR_E}{R}\right)^m$$

is used, where n_{eq} is the density on the equatorial plane, L is the magnetic L-shell parameter, R_E is Earth radius, R is geocentric distance to the observation point and m is the power-law index. The density profile for diffusive equilibrium is closed, having a low-m (m=0.5~1) power law distribution, whereas, the density profile for collisionless plasma corresponds to high-m (m~4) power law distributions (Eviatar et al., 1964; Angerami and Carpenter, 1966; Takahashi et al., 2004).

We have, however, few opportunities to investigate the field aligned profile of plasma density from actual observational data. Previous studies have been done using (i) in-situ measurements of electron density from plasma wave data by polar orbiting spacecraft (e.g., Goldstein et al., 2001; Denton et al., 2002; Sandhu et al., 2016), (ii) passive remote sensing of electron density with whistler waves (e.g., Angerami and Carpenter, 1966), (iii) passive remote sensing of plasma mass density with harmonic frequencies of standing Alfven waves in the ultra-low frequency (ULF) range (e.g., Takahashi et al., 2004; Denton et al., 2009), (iv) active remote sensing of electron density by the radio plasma imager (RPI) onboard the Imager for Magnetopause-to-Aurora Global Exploration (IMAGE) satellite (Reinisch et al., 2001; Huang et al., 2004).

Goldstein et al. (2001) used the electron density measurements of the Polar satellite and obtained a power-law index of $m = 0.37 \pm 0.8$ for high density regions (n_e>100/cc) and 1.7 ± 1.1 for low density regions (n_e<100/cc). Denton et al. (2002) used same data set as Goldstein et al. (2001) and estimated a power-law index of 1.6-2.1 for the plasmatrough. Takahashi et al. (2004) estimated the power-law index of

the plasma mass density and found that $m \sim 0.5$ at $4<L<6$, which is consistent with a diffusive equilibrium solution. On the other hand, no single value of m fit the average observed frequency ratios at $6<L<7$, and the theoretical solutions indicated that the mass density was peaked at the equator. The subsequent studies by Denton et al. (2009) and Sandhu et al. (2016) analyzed Cluster data and showed that the electron density also had a local maximum in density near the equator in the plasmatrough. As described above, many results have been obtained in which both electrons and ions have had a density distribution close to diffusion equilibrium as long as they have been in the high-density region in the plasmasphere. Also, in high L-shell regions with low density, power-law indices m have had larger values or have not tended to take a specific value, which implied that there may have been a local maximum in density near the equatorial plane.

In recent years, the exploration of the inner magnetosphere has entered the multi-point observation era with satellites flying in formation. In order to obtain a comprehensive understanding of the acceleration, transport, and loss of relativistic electrons in the radiation belts, cross-energy coupling of the inner magnetospheric plasma has been of prime interest. (Miyoshi et al., 2016; 2018a). To understand the detailed cross-energy coupling processes, it is necessary to know all parameters that contribute to the coupling. Despite the fact that the plasmasphere is the lowest energy population in the inner magnetosphere, it is also important, because it dominates the background plasma environment which controls wave dispersion and resonance conditions. Moreover, the latitudinal distribution of plasma density significantly controls propagations of plasma waves.

In this paper, we show simultaneous measurements of the plasma density along the same magnetic field by proposing a new method for examining the density profile along the magnetic field lines of plasma electron density at Arase (Exploration of energization and Radiation in Geospace: ERG) satellite (Miyoshi et al., 2018a) and Van Allen probes (the Radiation Belt Storm Probes: RBSP, Mauk et al., 2013) era. We estimate the power-law index of three events during and after the 7 September 2017 storm event using in-situ measurements of the electron number density from Arase and RBSP whose orbits have different inclinations. This gives instantaneous information about the density profile along field lines. Thus, it provides an opportunity to capture dynamic changes of the plasmasphere during magnetic storms.

2. Simultaneous Observations by Arase and RBSP-B

2.1. Satellite orbits

Figure 1 shows the positions of Arase (the red line with circles) and RBSP-B (the blue line with triangles) in the L-value-Magnetic Local Time (MLT) plane (top) and L-value-Magnetic Latitude plane (bottom) during the conjugate event on 8 Sep 2017 when the spacecraft pass the same L-value (L = 3.3-4.1). The exact time of the two orbits are indicated in the top panel. The small circles and triangles on the orbits respectively indicate every five-mins positions of Arase and RBSP-B. The L-value, MLT and magnetic latitude of the satellites were calculated by using Olson-Pfitzer-Quitet (OPQ 77) magnetic field model (Olson and Pfitzer, 1977), and the L-value is McIlwain L-parameter (McIlwain, 1961) for particles with a pitch angle of 90 degrees. Their orbits seem to cross in the afternoon sector. In fact, the difference of MLT and UT comparing at the same L-values are less than 0.5 hr and 15 mins, respectively. Such a conjunction event provides a good opportunity to compare the electron density between the two different latitudes due to the difference of inclinations of Arase and RBSP. As shown in the bottom panel of Figure 1, Arase was ~10 degrees higher in latitude than RBSP-B.

2.2. Evolution of the Plasmasphere during the 7 Sep 2017 Storm Event

The top and middle panels of Figure 2 respectively display temporal variations of the Kp and SYM-H indices during the interval of 6-10 Sep 2017. They indicate that a magnetic storm with two main phases commenced around 0 UT on 8 Sep and disturbances continued for approximately 30 hrs, followed by a gradual recovery phase. This storm has been considered to be a CME (coronal mass ejection)-driven storm. The blue, green, black and magenta bars in the middle panel indicate the time intervals when the electron density, shown in the bottom panel of this figure were observed. The event numbers in parentheses are the event numbers defined in Sections 2-3, 2-4 and 2-5.

A detailed description of the plasmaspheric dynamics during this storm event is given by Obana et al. (2019), therefore, here we give only a brief description. The bottom panel of Figure 2 shows L-value distribution of electron density obtained by the Arase observations. The exact times are given in the panel. The blue line (0) indicates a plasmasphere which spreads to L ~5 before the storm. The green line (1) shows that the plasmasphere has eroded to L=2.5 during the second main phase. In L >3 of the green line profile, the density shows jagged structures. It implies that the satellite was in the plasmatrough with variations in electron density. In black (2), the plasmasphere has been extremely eroded and the plasmapause reached around L = 1.6-1.7. An isolated increase in density appears to be a plume at L = 3.4-4.3. The magenta line (3) was obtained two days after the magnetic storm entered the second

recovery phase, and the eroded plasmasphere has partially refilled.

2.3. Event #1: 23:20 UT on 8 Sep 2017

Figure 3 shows the plasma wave observations from Arase and RBSP-B and locations of the satellites during 23:20 UT on 8 Sep – 00:10 UT on 9 Sep 2017. Figure 3a is the plasma wave spectrogram for the electric field in the frequency range of 10-400 kHz measured by the onboard frequency analyzer (OFA) and the high-frequency analyzer (HFA) of the Plasma Wave Experiment (PWE) (Kasahara et al., 2018; Kumamoto et al., 2018). The clear emissions of the Upper Hybrid Resonance (UHR) waves is identified by the white line and arrow. The UHR frequency was decreasing gradually from 300 to 100 kHz during 23:20-23:48 UT because Arase was in an outbound pass, and then suddenly jumped up to ~150 kHz at 23:49 UT. This implies that the satellite passed the boundary between the low- and high-density regions, which correspond to the inner trough and plasma plume, respectively.

Figure 3b shows the plasma wave spectrogram for electric fields for RBSP-B. These data were measured by the Electric and Magnetic Field Instrument Suite and Integrated Science (EMFISIS) Wave instrument (Kletzing et al., 2013). The UHR waves can be seen as indicated by the white line and arrow and its frequency gradually increased since RBSP-B was in an inbound pass. Its frequency raised in stepwise fashion at 23:21 UT and decreased around 23:50 UT. This implies that the satellite passed the plume and came into the inner trough around 23:50 UT.

Figure 3c-e respectively show the L-value, MLT and magnetic latitude of Arase (the red line) and RBSP-B (the blue line). They are calculated using the OPQ77 magnetic field model, because this time interval is in the recovery phase of the storm. The thick parts of the lines indicate each value as the satellites passed L=3.3-4.1. In this L-value range, the two satellites passed the points with same L-values with time differences of less than 30 mins. The differences in MLT between Arase and RBSP-B were less than 0.5 hr. Due to the difference of inclinations, the magnetic latitudes of Arase were ~10 degrees higher than that of RBSP-B.

From the upper-limit frequency of the UHR waves (f_{UHR}), the electron density n_e along the spacecraft orbit is estimated using the following equation

$$n_e = \frac{{f_{UHR}}^2 - {f_{ce}}^2}{8980^2},$$

where f_{ce} is the electron cyclotron frequency. The densities and frequencies are expressed in cubic centimeters and in hertz, respectively. In this paper, the local f_{ce} was calculated from the spin average total magnetic field intensity measured by

the Magnetic Field Experiment (MGF) instrument (Matsuoka et al., 2018) onboard Arase or the EMFISIS magnetometer onboard RBSP.

The upper panel of Figure 4 shows the electron number density profiles as a function of L. A density jump can be seen around L~3.45 in the Arase observations (red) and around L~3.57 in the RBSP-B observations (blue), respectively. These jumps correspond to the boundary between the inner trough and plume. The difference in the L-values of the boundaries between Arase and RBSP-B may be due to the difference of MLT of the satellites.

Interestingly, the two satellites differed in magnetic latitude by as much as 10 degrees, but in the plume, n_e shows similar values at same L-values. That is, the density of the plume seems to be almost uniform at least in the magnetic latitude range of 10-30°. Whereas in the inner trough, the n_e at higher latitudes (Arase) is higher. That is, the n_e changes rather steeply along the field line.

Assuming a power-law density distribution as function of geocentric distance, the power-law index m can be calculated as

$$m = -\frac{\ln(n_{e1}/n_{e2})}{\ln(R_1/R_2)}$$

and shown in the lower panel of Figure 4. Where the subscripts "1" and "2" indicate values for satellites #1 and #2. For this calculation, moving averages of n_e with a 0.05 of window width in L-value were used. The m index is plotted in the panel only if both relative standard deviations (the ratio of the standard deviation to the average) of n_e of Arase and RBSP-B in the window are less than 25 %. The m indices were 4 to 7 and -3 to 0 in the inner trough and plume, respectively. These are indicated in the lower panel of Figure 4.

2.4. Event #2: 14:15 UT on 8 Sep 2017

Figure 5 shows the plasma wave observations and locations of Arase and RBSP-B during the interval 14:15-15:05 UT on 8 Sep 2017, in the same format as Figure 3, but L-value, MLT and magnetic latitude are calculated using the Tsyganenko 2004 storm time model (TO4s, Tsyganenko and Sitnov, 2005), because this period is in the second main phase of the storm. The clear emissions of the UHR waves are found as shown by the white lines and arrows. The UHR frequency fluctuates with the time scale of the range from 1 to 10 min. The timing of the fluctuations seems to be inconsistent between the two satellites, thus, it is surmised that this change in frequency does not reflect the time change of the electron density, but reflects the spatial variation. As shown in Figure 2, this observation is during the second main phase, with a plasmapause

seen at L=2.5, thus, the fluctuations of f_{UHR} shown in Figure 5 implies existence of small-scale structures in the plasmatrough.

Results showing this expectation are given in Figure 6. The upper panel of Figure 6 shows the electron number density profiles as a function of the McIlwain's L-parameter calculated using the T04s model during Event #2. At least between L = 3.3 and 3.9, the changes in electron density observed by Arase and RBSP-B seem to be correlated.

Using ~10 degrees as the difference in magnetic latitudes (Figure 5e), the m index was calculated as shown in the bottom panel of Figure 6. In both the high- and low-density regions, the derived m index has small values (typically ~0). Obviously, the very large negative values for L>3.9 are meaningless, because the fluctuations in electron densities observed by Arase and RBSP-B are not correlated each other in this region.

2.5. Event #3: 13:40 UT on 10 Sep 2017

The third event is a conjunction of Arase and RBSP-A, during the interval of 13:40-14:30 UT on 10 Sep, in the recovery phase of the storm. Figure 7 (same format as Figure 3) shows a simple picture of emission. The f_{UHR} observed by Arase gradually decreased from 200 to 70 kHz, and those observed by RBSP-A gradually increased from 100 to 200 kHz. This corresponds to the gradual electron density gradient with distance. The time of this event is about two days after the commencement of the second recovery phase, thus the observations depict the density profiles of a partially refilled plasmasphere (Figure 2).

Figure 8 shows the n_e obtained by Arase and RBSP-A observations (upper) and the inferred m index (bottom) in the same format as Figure 4. Interestingly, the electron density observed by RBSP-A was higher than that by Arase, despite RBSP-A being at a lower latitude. Because plasmaspheric plasma is supplied from the underlying ionosphere, the density is usually lower in near the equator. However, our results suggest a profile opposite to this. The bottom panel of Figure 8 shows m index, which has negative values due to the higher electron density near the equator.

3. Discussion.

3.1. Accuracy and coverage of this study

The three conjunction events shown in this study have <45 mins difference in UT and <1 hr difference in MLT when the two satellites cross flux tubes with same L-value. The L-value includes an uncertainty of 0.05 derived from the window width used for

279 the moving average of n_e.
280 Comparing to previous studies, IMAGE-RPI sounding takes only two minutes to make
281 one survey (Song et al., 2005). On the other hand, studies using polar orbiting
282 satellites, take several hours until the satellite passes two points of the flux tube
283 with the same L-value (Goldstein et al.,2001). Our surveys have time accuracies
284 intermediate to those studies.
285 Next, we compare our time accuracies with the time scale of dynamic changes of
286 the plasmasphere. According to Obana et al. (2010), the refilling rates at L = 3.8
287 were estimated to be 13 amu/cm^3/hr, so assuming that all the ions are protons, the
288 electron density will increase 10/cm^3 in 45 mins. Even in low-density regions (n_e~100
289 /cm^3), this is only a 10% increase in density. On the other hand, Goldstein et al.
290 (2003) investigated images of the He^+ plasmasphere taken by the IMAGE-EUV camera and
291 reported that the nightside plasmapause had moved inward by ~2 R_E in 3 hrs during the
292 erosion. In such a case, density changes more quickly, and thus, more precise
293 conjunctions (with shorter time differences) will be required.
294 The difference in MLT must be considered when structures that change in both radial
295 and azimuthal directions, like the plume, are considered. In fact, as shown in Figure
296 4, the position of the inner edge of the plume observed by Arase and RBSP were displaced
297 by 0.12 R_E. This may be due to the difference in MLT.
298 The coverage of magnetic latitudes should also be considered. The satellites used
299 in this study explore magnetic latitudes of < 30 degrees (Arase) and <10 degrees (RBSP).
300 Note that the m indices presented in this study do not represent the entire magnetic
301 field line, but only in this range.
302
303 **3.2. Power-law index for the inner trough and the plume**
304 In Event #1, the power-law index shows respectively m >4 at L=3.3-3.4 (inner
305 trough), and m ~0 at L=3.6-4.1 (plume). This is interpreted as the inner trough being
306 close to collisionless and the plume being near diffusive equilibrium. Previous
307 studies explained that the plume and inner trough are formed by the convection electric
308 field which cause sunward motion of the plasma, the subsequent corotation and the
309 subauroral polarization stream (SAPS) electric field. Based on this idea, the plumes
310 originate in the main body of the plasmasphere and inner troughs originate in the
311 low-density region (so-called outer trough) after the plasmasphere shrank. Our
312 results do not conflict with this model.
313
314 **3.3. Negative power law index in the partial refilling region**

In Event #3, power-law index m shows negative values, meaning that the density in the equatorial plane is higher than off the equator. The plasmaspheric density is generally higher closer to Earth. This reflects that the plasma is of ionospheric origin. However, the electron density in Event #3 shows the opposite features. How can these results be explained?

The period of Event #3 is about two days after of the commencement of the second recovery phase, and the flux tubes had been partially refilled. When the upper ionosphere comes into the sunlight, plasma is supplied through photoionization. So, if the length of time after sunrise is different between the flux tubes at Arase and RBSP, the density may be different. However, as shown in Figure 7d, the MLT is almost same for each L-shells, this effect seems unlikely.

Another possibility is the time difference from the end of the main phase. As shown in Figure 7c, the time differences between when the two satellites cross the same L-shells are 0-45 mins. According to the estimate in section 3.1, n_e can increase 0-10/cm^3 for such intervals. This effect is too small to interpret the high n_e at the equator. So, we conclude that this difference in density was real, and that there was an increase in density near the equator. Sandhu et al. (2016) statistically analyzed Cluster data and found that the electron density had a localized increase in density near the equator of the plasmatrough. Perhaps even in the partially refilled plasmasphere, the increase in density near the equator may be a common phenomenon. This is an important issue for future research.

3.4. Application for the Remote Sensing Plasma Mass Density

Standing field line resonances (FLRs) in the ULF frequency range are ubiquitous in the magnetosphere, and the frequency of FLRs (f_{FLR}) provides an opportunity to remotely sense the plasma mass density (e.g., Obayashi and Jacobs, 1958; Kitamura and Jacobs, 1968). The procedure for estimating the plasma mass density from the f_{FLR} is to (i) obtain the f_{FLR} from the observation data, (ii) choose a suitable magnetic field model, (iii) select a suitable model for the variation of the plasma mass density along the field line, and (iv) solve the FLR wave equation for the plasma mass density. However, there is very little information about the variation of the density along the field line. Our analysis method makes it possible to obtain this information in the Arase-RBSP era and contributes to the improvement of the accuracy of mass density estimates from the f_{FLR}.

4. Summary

Using plasma waves observed by Arase and RBSP-A and B, we estimated the power-law index m for the field-aligned distributions of n_e for flux tubes at L=3.3-4.1. During and after the 7 Sep 2017 storm event, three conjunction events were studied, in which differences of MLT and UT were respectively <1 hr and <45 mins. In the plume, n_e had comparable values at the higher and the lower latitudes, and the m index was estimated to be ~0. This density profile is expected for diffusive equilibrium. On the other hand, in the inner trough, n_e off the equator was higher than that at near equator, and the m index was estimated as 4-7. Plasma in this region seems to be collisionless. When the satellites were in the plasmatrough with variable n_e, values of n_e off the equator and near the equator were similar; the m index was estimated to be ~0 for both high- and low-density regions. This implies that the plasma transport process might be different between the low-density regions in the variable density structure and the inner trough. In the partially refilled plasmasphere, n_e near the equator was higher than off the equator. This suggests the existence of plasma concentration around the equator.

Acknowledgement

This work was supported by JSPS KAKENHI Grants 15H05815, 15H05747, 16H04057, 17H00728, 19H01958 and 20H01959. The work at the University of Iowa is supported by NASA through JHU/APL contract 921647 under NASA's prime contract No. NAS5-01072.

Science data of the ERG (Arase) satellite were obtained from the ERG Science Center operated by ISAS/JAXA and ISEE/Nagoya University (https://ergsc.isee.nagoya-u.ac.jp/index.shtml.en; Miyoshi et al., 2018b). The present study analyzed PWE-HFA-L2 V01_01, MGF-L2 V03.03, and OBT L2 v02 data.

The Van Allen Probes/EMFISIS data are available at http://emfisis.physics.uiowa.edu. The present study used the EMFISIS-L2 v1.6.3 data. We thank the EMFISIS team for providing the EMFISIS data.

The solar wind parameters are obtained from the NASA OMNI website (https://omniweb.gsfc.nasa.gov/). We acknowledge use of NASA/GSFC's Space Physics Data Facility's OMNIWeb service and OMNI data.

Figure Captions

Figure 1. The positions of Arase (red line) and RBSP-B (blue line) during the interval of 23:30–24:00 UT on 8 Sep 2017 in the L-value- Magnetic Local Time (MLT) plane (top) and L value-Magnetic latitude plane (bottom). The top panel shows exact times of each of the orbits. The small circles and triangles on the orbits respectively indicate positions every five mins of Arase and RBSP-B. Their orbits cross in the afternoon sector. In fact, the difference of MLT and UT comparing at the same L-values are less than 0.5 hr and 15 mins, respectively. Such a conjunction event a gives significant opportunity to compare the electron density between the two different latitudes due to the difference of inclinations of Arase and RBSP.

Figure 2. This figure shows the overall picture of the 7 Sep 2017 storm event and Arase observations shown in this paper. The temporal variations of the Kp and SYM-H indices during the interval from 6–10 Sep 2017 are shown in the top and middle panels, respectively. The blue, green, black, and magenta bars in the middle panel indicate the time intervals when the electron densities shown in the bottom panel were observed. The event numbers in parentheses are the event numbers defined in Sections 2-3, 2-4 and 2-5. Arase observations of cold electron density profiles as a function of the McIlwain L-parameter are shown in the bottom panel. The exact times of each observation are provided within the panel. All observations are from outbound orbits. Blue (0): expanded plasmasphere before the storm, extending to L=4.8–5.0. Green (1): the plasmapause pushed further earthward at L=2.5 immediately after the second main phase. Black (2): the severely eroded plasmasphere with the plasmapause being pushed even further at L=1.6–1.7. Magenta (3): partial recovery of the severely eroded plasmasphere at 1.5 days after density profile #2 (black).

Figure 3. Spectrograms of radio and plasma waves obtained by Arase (a) and RBSP-B (b) from 23:20 UT on 8 Sep to 00:10 UT on 9 Sep 2017. In both panels, narrow-banded UHR waves are clearly found and indicated by the white lines and arrows. In 3a, the UHR frequency was decreasing gradually from 300 to 100 kHz during 23:20–23:48 UT because Arase was in an outbound pass, and then suddenly jumped up to ~150 kHz at 23:49 UT. This implies that the satellite passed the boundary between low- and high-density regions, which correspond to the inner trough and plasma plume, respectively. In 3b, The observation time is divided into a period showing the high UHR frequency before 23:52 UT and a period showing a low UHR frequency after 23:52 UT. Each corresponds to the times the satellite flying into the high-density plume and the low-density inner trough. The lower three panels show L-value (c), magnetic local time (MLT) (d), and magnetic latitudes (e) of Arase and RBSP-B. They are calculated using the Olson-Pfitzer-Quitet (OPQ 77) magnetic field model (Olson and Pfitzer, 1977). The thick portion of the lines indicate the position of the satellite orbits when their L-values are in the range of L=3.3–4.1. The time is 23:46–23:59 UT

for Arase and 23:31–24:00 UT for RBSP-B.

Figure 4. (top) L-value profile of the electron density inferred from f_{UHR} using the plasma wave observations during 23:30–24:00 UT on 8 Sep 2017. The red and blue dots indicate Arase and RBSP-B observations, respectively. (bottom) L-value profile of the power-law index *m* (defined in Section 2.3) which is estimated using differences of electron density and magnetic latitude between Arase and RBSP-B.

Figure 5. Spectrograms of radio and plasma waves obtained by Arase (a) and RBSP-B (b), L-value (c), magnetic local time (MLT) (d) and magnetic latitude (e) of Arase and RBSP-B during 14:15-15:05 UT on 8 Sep 2017. The locations of the satellites are computed by using the Tsyganenko 2004 storm model. The format of this figure is same as that of Figure 3. The UHR frequency fluctuates with a time scale in the range from 1 to 10 mins. This observation is during the second main phase, with the plasmapause seen at L=2.5, thus, the fluctuations of f_{UHR} imply existence of small-scale structures in the plasmatrough.

Figure 6. (top) L-value profiles of the electron density inferred from f_{UHR} using the plasma wave observations during 14:15–15:05 UT on 8 Sep 2017. The red and blue dots indicate Arase and RBSP-B, respectively. (bottom) L-value profile of the power-law index *m* which is estimated using differences of electron density and magnetic latitude between Arase and RBSP-B. Between L=3.3 and 3.9, the changes in electron density observed by two satellites seems to be correlated, thus the *m* index ~0 in both the high- and low-density regions.

Figure 7. Spectrograms of radio and plasma waves obtained by Arase (a) and RBSP-B (b), L-value (c), magnetic local time (MLT) (d), and magnetic latitude (e) of Arase and RBSP-B during 13:40–14:30 UT on 10 Sep 2017. The locations of the satellites are computed using OPQ 77 model. The format of this figure is same as that of Figure 3. The f_{UHR} observed by Arase (RBSP-A) gradually decreased (increased). This corresponds to the gradual electron density gradient with distance in the plasmasphere.

Figure 8. L-value profiles of the electron density and the power-law index *m* during 13:40–14:30 UT on 10 Sep 2017. The format of this figure is same as that of Figure 4. Due to the limits of the frequency resolution of the spectrogram shown by Figure 7b, the RBSP-B observations are aligned in a stepped shape. The time of this event is about two days after the commencement of the second recovery phase of the storm, thus the observations depict the density profiles of a partially refilled

plasmasphere. The negative values of *m* index indicate higher electron density at near the equator than that off the equator.

References

Angerami, J. J., and D. L. Carpenter (1966), Whistler studies of the plasmapause in the magnetosphere: 2. Electron density and total tube electron content near the knee in the magnetospheric ionization, J. Geophys. Res., 71, 711-725.

Denton, R. E., J. Goldstein, J. D. Menietti, and S. L. Young (2002), Magnetospheric electron density model inferred from Polar plasma wave data, J. Geophys. Res., 107, 1386, doi:10.1029/2001JA009136.

Denton, R. E., et al. (2009), Field line distribution of density at L = 4.8 inferred from observations by CLUSTER, Ann. Geophys., 27, 705-724, doi:10.5194/angeo-27-705-2009.

Eviatar, A., Lenchek, A. M., & Singer, S. F. (1964). Distribution of Density in an Ion-Exosphere of a Nonrotating Planet. The Physics of Fluids, 7(11), 1775-1779. https://doi.org/10.1063/1.2746776.

Goldstein, J., R. E. Denton, M. K. Hudson, E. G. Miftakhova, S. L. Young, J. D. Menietti, and D. L. Gallagher (2001), Latitudinal density dependence of magnetic field lines inferred from Polar plasma wave data, J. Geophys. Res., 106, 6195-6202, doi:10.1029/2000JA000068.

Goldstein, J., B. R. Sandel, W. T. Forrester, and P. H. Reiff, IMF-driven plasmasphere erosion of 10 July 2000, Geophys. Res. Lett., 30(3), 1146, doi:10.1029/2002GL016478, 2003.

Huang, X., B. Reinisch, P. Song, J. L. Green, D. L. Gallagher (2004), Developing an empirical density model of the plasmasphere using IMAGE/RPI observations, Advances in Space Research, 33(6):829-832, DOI: 10.1016/j.asr.2003.07.007.

Kasahara, Y., Kasaba, Y., Kojima, H., Yagitani, S., Ishisaka, K., Kumamoto, A., et al. (2018). The Plasma Wave Experiment (PWE) onboard the Arase (ERG) satellite. Earth,

Planets and Space, 70(1), 86. https://doi.org/10.1186/s40623-018-0842-4

Kletzing, C. A., Kurth, W. S., Acuna, M., MacDowall, R. J., Torbert, R. B., Averkamp, T., et al. (2013). The Electric and Magnetic Field InstrumentSuite and Integrated Science (EMFISIS) on RBSP. Space Science Reviews, 179(1-4), 127-181. https://doi.org/10.1007/s11214013-9993-6

Kumamoto, A., Tsuchiya, F., Kasahara, Y., Kasaba, Y., Kojima, H., Yagitani, S., et al. (2018). High Frequency Analyzer (HFA) of Plasma Wave Experiment (PWE) onboard the Arase spacecraft. Earth, Planets and Space, 70(82). https://doi.org/10.1186/s40623-018-0854-0

Matsuoka A, Teramoto M, Nomura R, Nose M, Fujimoto A, Tanaka Y, Shinohara M, Nagatsuma T, Shiokawa K, Obana Y, Miyoshi Y, Mita M, Takashima T, Shinohara I (2018) The Arase (ERG) magnetic field investigation. Earth Planets Space 70:43. https://doi.org/10.1186/s40623-018-0800-1

Mauk, B. H., Fox, N. J., Kanekal, S. G., Kessel, R. L., Sibeck, D. G., & Ukhorskiy, A. (2013). Science objectives and rationale for the Radiation Belt Storm Probes Mission. Space Science Reviews, 179(1-4), 3-27. https://doi.org/10.1007/s11214-012-9908-y.

McIlwain, C. E. (1961). Coordinates for mapping the distribution of magnetically trapped particles. Journal of Geophysical Research, 66(11), 3681-3691. https://doi.org/10.1029/JZ066i011p03681

Miyoshi Y, Ono T, Takashima T, Asamura K, Hirahara M, Kasaba Y, Matsuoka A, Kojima H, Shiokawa K, Seki K, Fujimoto M, Nagatsuma T, Cheng CZ, Kazama Y, Kasahara S, Mitani T, Matsumoto H, Higashio N, Kumamoto A, Yagitani S, Kasahara Y, Ishisaka K, Blomberg L, Fujimoto A, Katoh Y, Ebihara Y, Omura Y, Nose Hori T, Miyashita Y, Tanaka Y-M, Segawa, ERG working group (2012) The energization and radiation in geospace (ERG) project. In: Summers D, Mann IR, Baker DN, Schulz M (eds) Dynamics of the Earth's radiation belts and inner magnetosphere. American Geophysical Union, Washington. https://doi.org/10.1029/2012gm001304

Miyoshi Y, Kataoka R, Ebihara Y (2016) Flux enhancement of relativistic electrons

associated with substorms. In: Balasis G, Daglis IA, Mann IR (eds) Waves, particles, and storms in geospace. Oxford Press, Oxford, pp 333-353

Miyoshi, Y., Shinohara, I., Takashima, T., Asamura, K., Higashio, N., Mitani, T., et al. (2018a). Geospace Exploration Project ERG. Earth, Planets and Space, 70(1), 101. https://doi.org/10.1186/s40623-018-0862-0

Miyoshi, Y., Hori, T., Shoji, M., Teramoto, M., Chang, T. F., Segawa, T., et al. (2018b). The ERG Science Center. Earth, Planets and Space, 70(1), 96. https://doi.org/10.1186/s40623-018-0867-8

Obana, Y., F. W. Menk, and I. Yoshikawa (2010), Plasma refilling rates for L = 2.3-3.8 flux tubes, J. Geophys. Res., 115, A03204, doi:10.1029/2009JA014191.

Obana, Y., Maruyama, N., Shinbori, A., Hashimoto, K. K., Fedrizzi, M., Nosé, M., et al. (2019). Response of the ionosphere-plasmasphere coupling to the September 2017storm: What erodes the plasmasphere so severely?, Space Weather, 17. https://doi.org/10.1029/ 2019SW002168

Olson, W. P., and K. A. Pfitzer, Magnetospheric magnetic field modeling, Annual Scientific Report, AFOSR Contract No. F44620-75-C-0033, 1977.

Reinisch, B. W., X. Huang, P. Song, G. S. Sales, S. F. Fung, J. L. Green, D. L. Gallagher, and V. M. Vasyliunas (2001), Plasma Density Distribution Along the Magnetospheric Field: RPI Observations From IMAGE, Geophys. Res. Lett., 28, 24, 4521-4524, doi:10.1029/2001GL013684.

Sandhu, J. K., T. K. Yeoman, R. C. Fear, and I. Dandouras (2016), A statistical study of magnetospheric electron density using the Cluster spacecraft, J. Geophys. Res. Space Physics, 121, 11,042-11,062, doi:10.1002/2016JA023397.

Song, P., B. W. Reinisch, X. Huang, J. L. Green (2005), 'Magnetospheric Active Wave Measurements', COSPAR Colloquia Series, Volume 16, Frontiers in Magnetospheric Plasma Physics: Celebrating 10 Years of Geotail Operation, pp. 235-246, doi.org/10.1016/S0964-2749(05)80036-8.

562 Takahashi, K., R. E. Denton, R. R. Anderson, and W. J. Hughes (2004), Frequencies
563 of standing Alfve´n wave harmonics and their implication for plasma mass distribution
564 along geomagnetic field lines: Statistical analysis of CRRES data, J. Geophys. Res.,
565 109, A08202, doi:10.1029/2003JA010345.
566
567 Tsyganenko, N. A. and Sitnov, M. I.: Modelling the dynamics of the inner magnetosphere
568 during strong geomagnetic storms, J. Geophys. Res., 110, A03208,
569 doi:10.1029/2004JA010798, 2005.
570

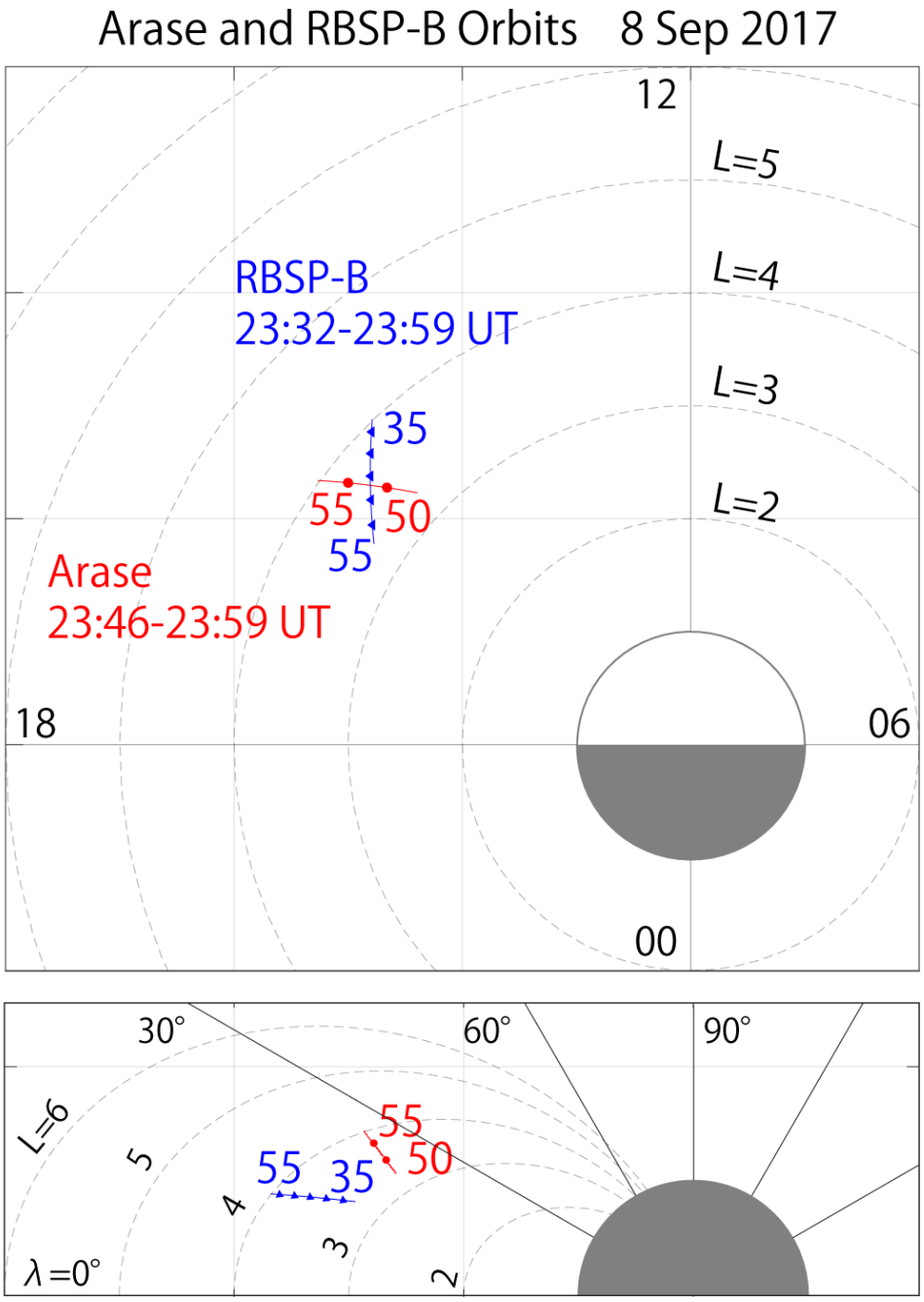

571

572 Figure 1

573

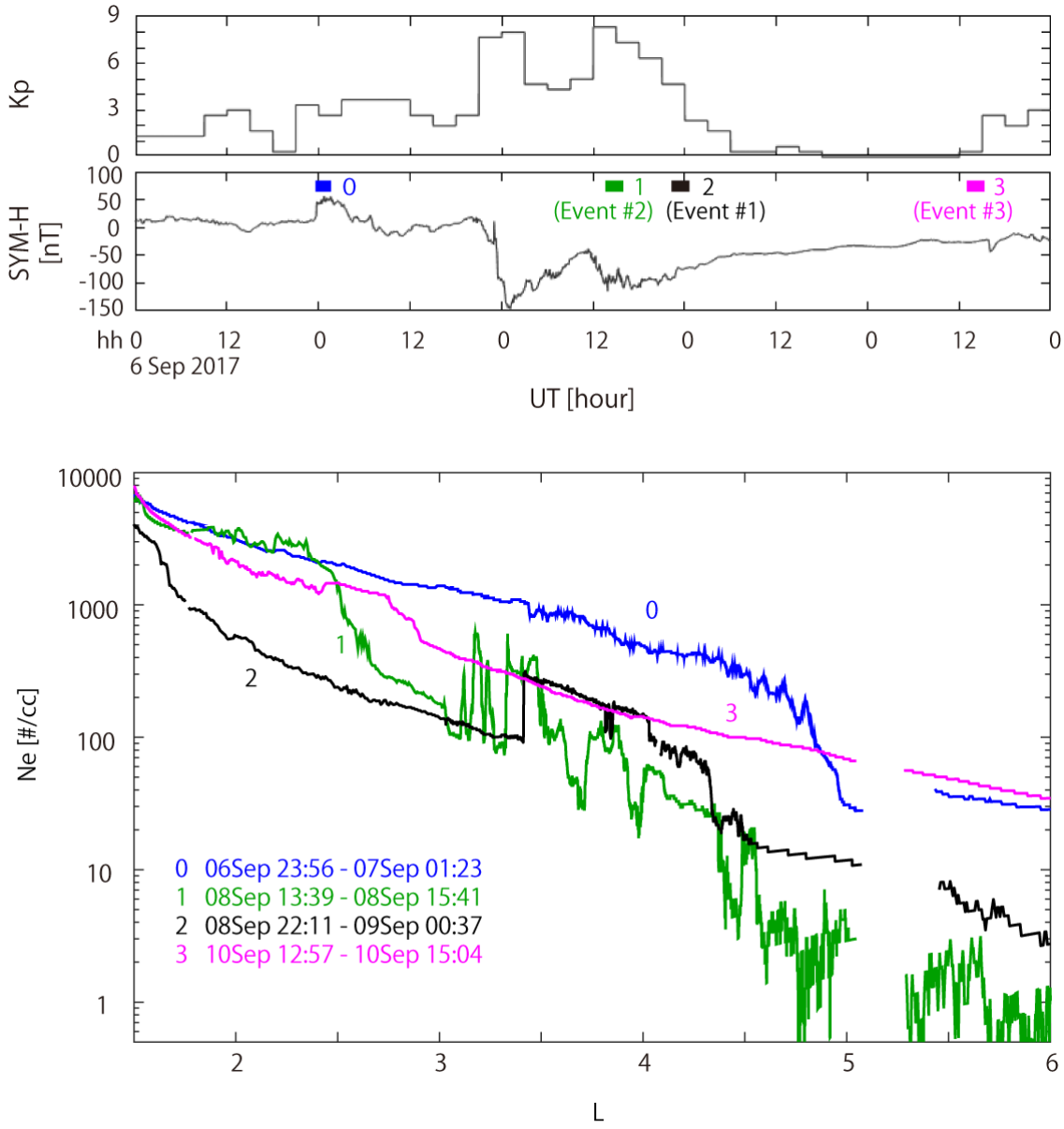

574

575

576

577

578

579 Figure 2

580

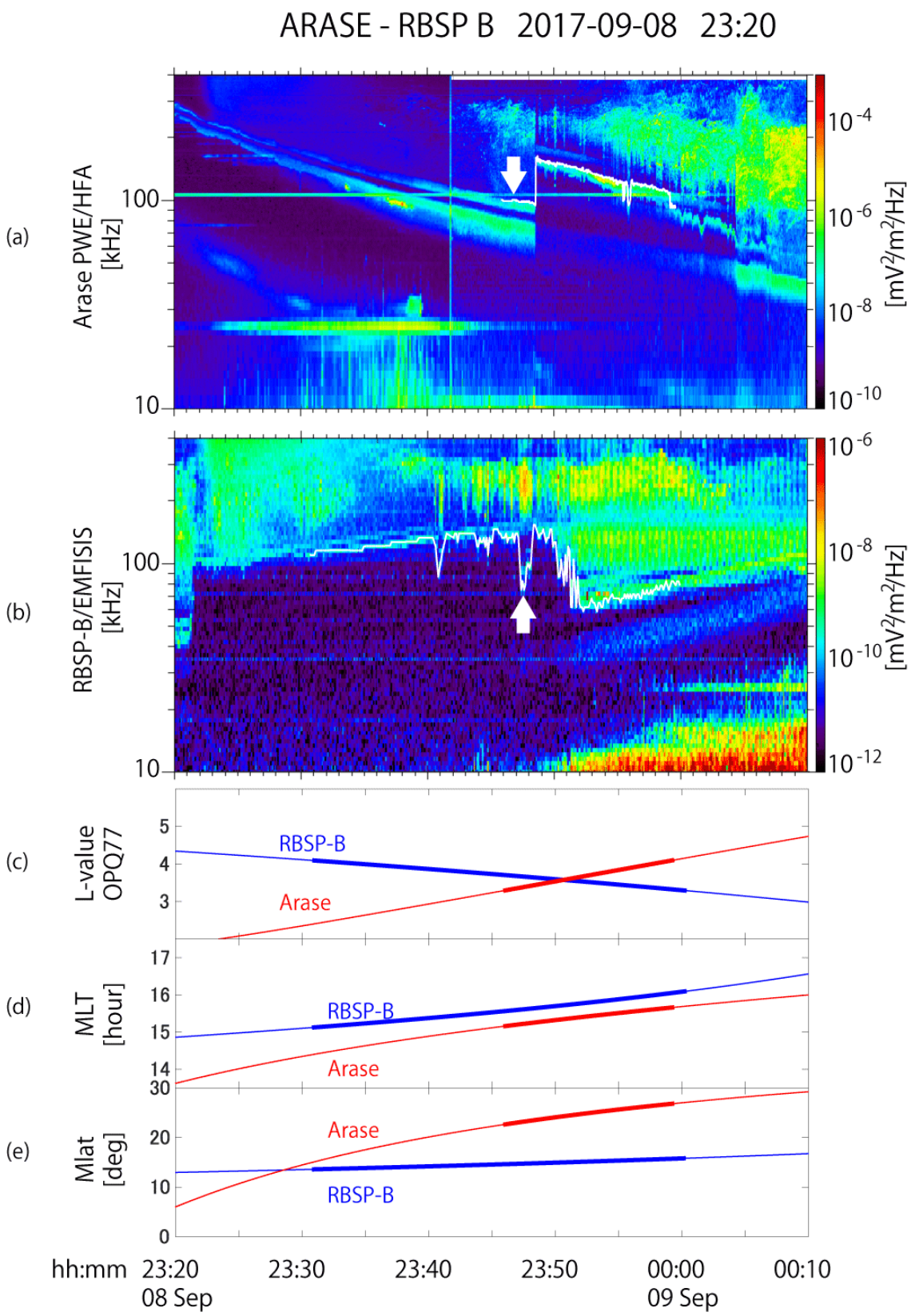
ARASE - RBSP B 2017-09-08 23:20
(a)
Arase PWE/HFA [kHz]
100
10
10^{-4}
10^{-6}
10^{-8}
10^{-10}
[mV²/m²/Hz]
(b)
RBSP-B/EMFISIS [kHz]
100
10
10^{-6}
10^{-8}
10^{-10}
10^{-12}
[mV²/m²/Hz]
(c)
L-value OPQ77
5
4
3
RBSP-B
Arase
(d)
MLT [hour]
17
16
15
14
RBSP-B
Arase
(e)
Mlat [deg]
30
20
10
0
Arase
RBSP-B
hh:mm
23:20
08 Sep
23:30
23:40
23:50
00:00
09 Sep
00:10

Figure 3

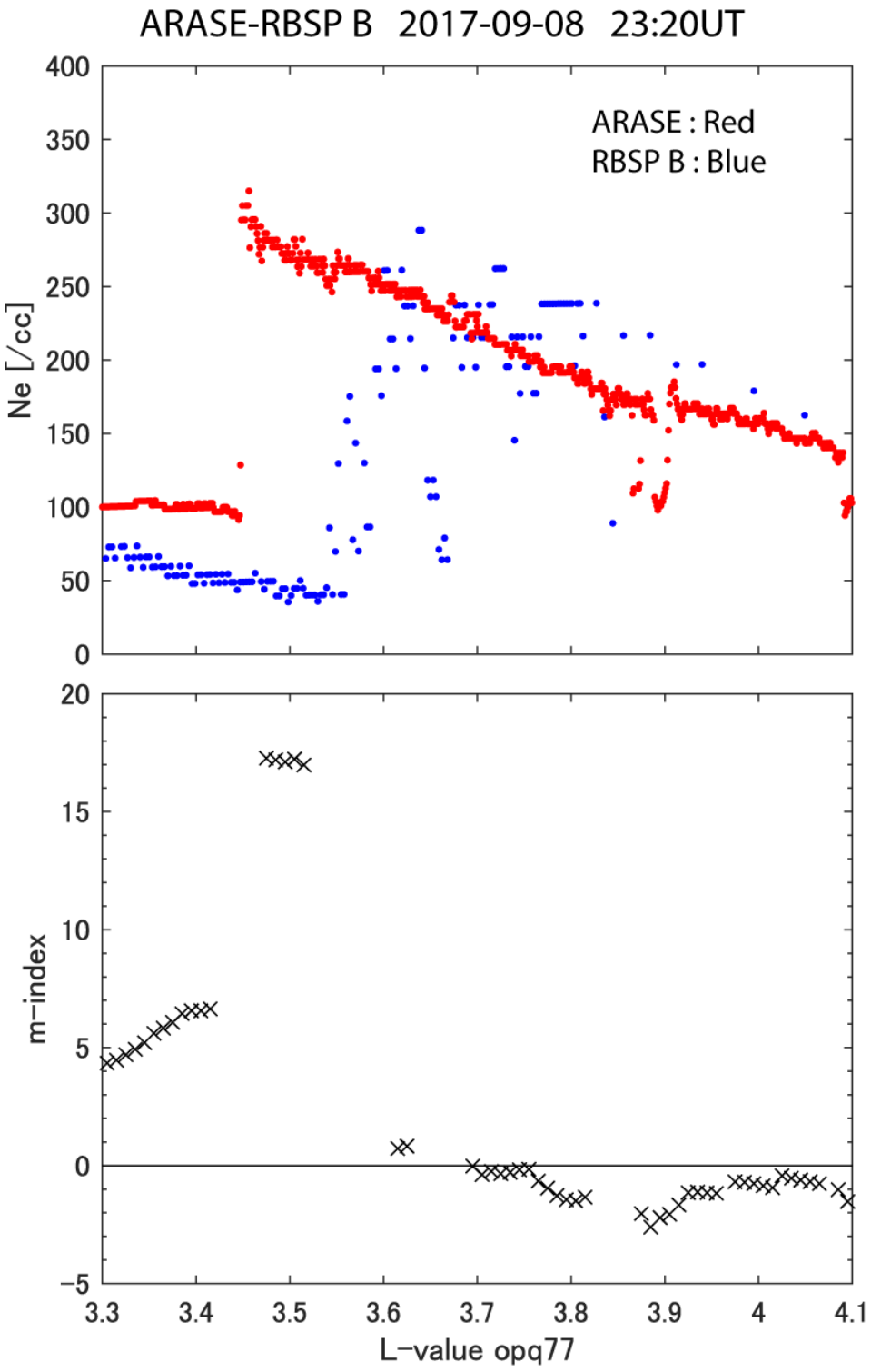

584

585

586 Figure 4

587

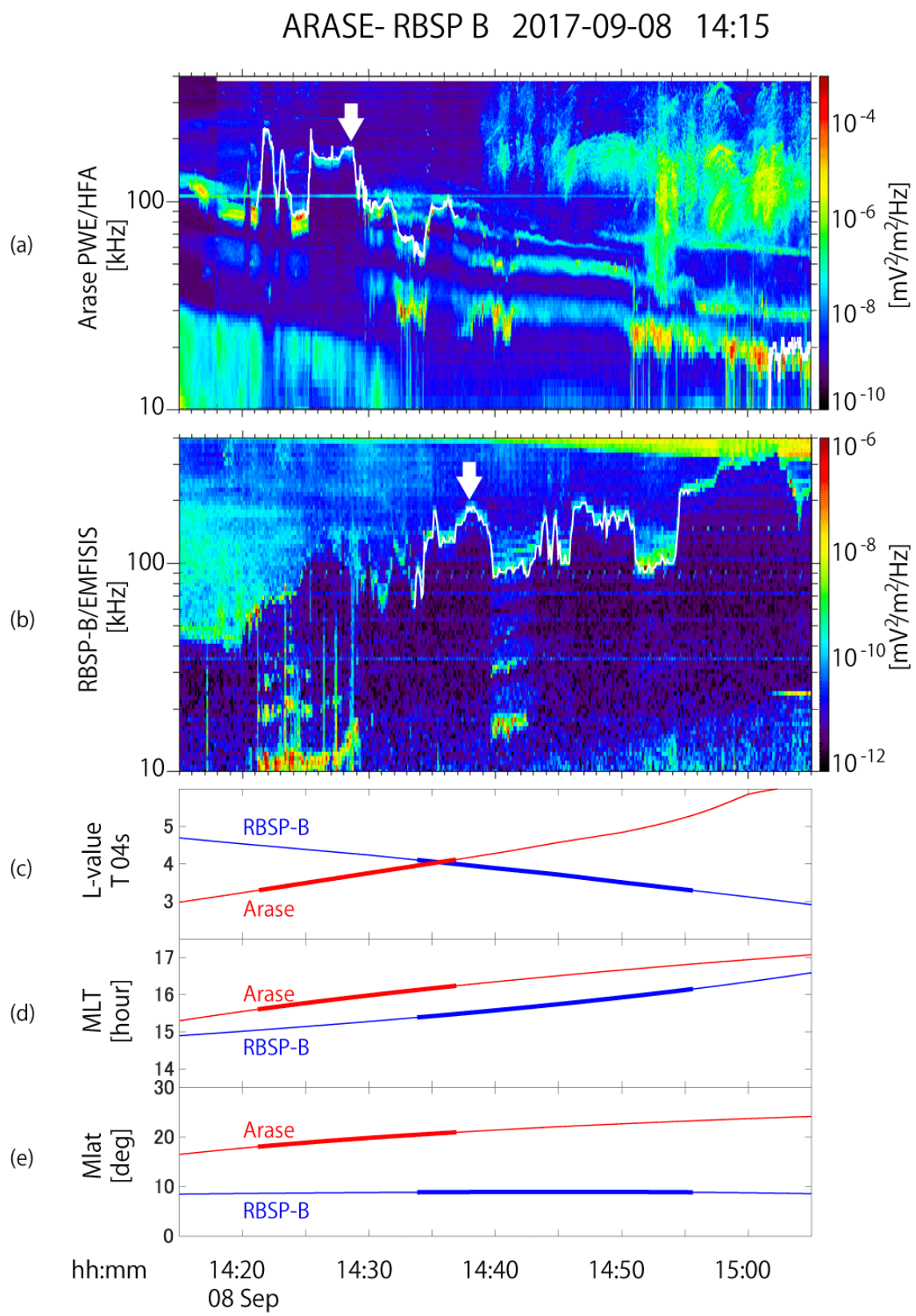
ARASE- RBSP B 2017-09-08 14:15
(a)
Arase PWE/HFA [kHz]
100
10
10^-4
10^-6
10^-8
10^-10
[mV²/m²/Hz]
(b)
RBSP-B/EMFISIS [kHz]
100
10
10^-6
10^-8
10^-10
10^-12
[mV²/m²/Hz]
(c)
L-value T04s
5
4
3
RBSP-B
Arase
(d)
MLT [hour]
17
16
15
14
Arase
RBSP-B
(e)
Mlat [deg]
30
20
10
0
Arase
RBSP-B
hh:mm
14:20
08 Sep
14:30
14:40
14:50
15:00

Figure 5

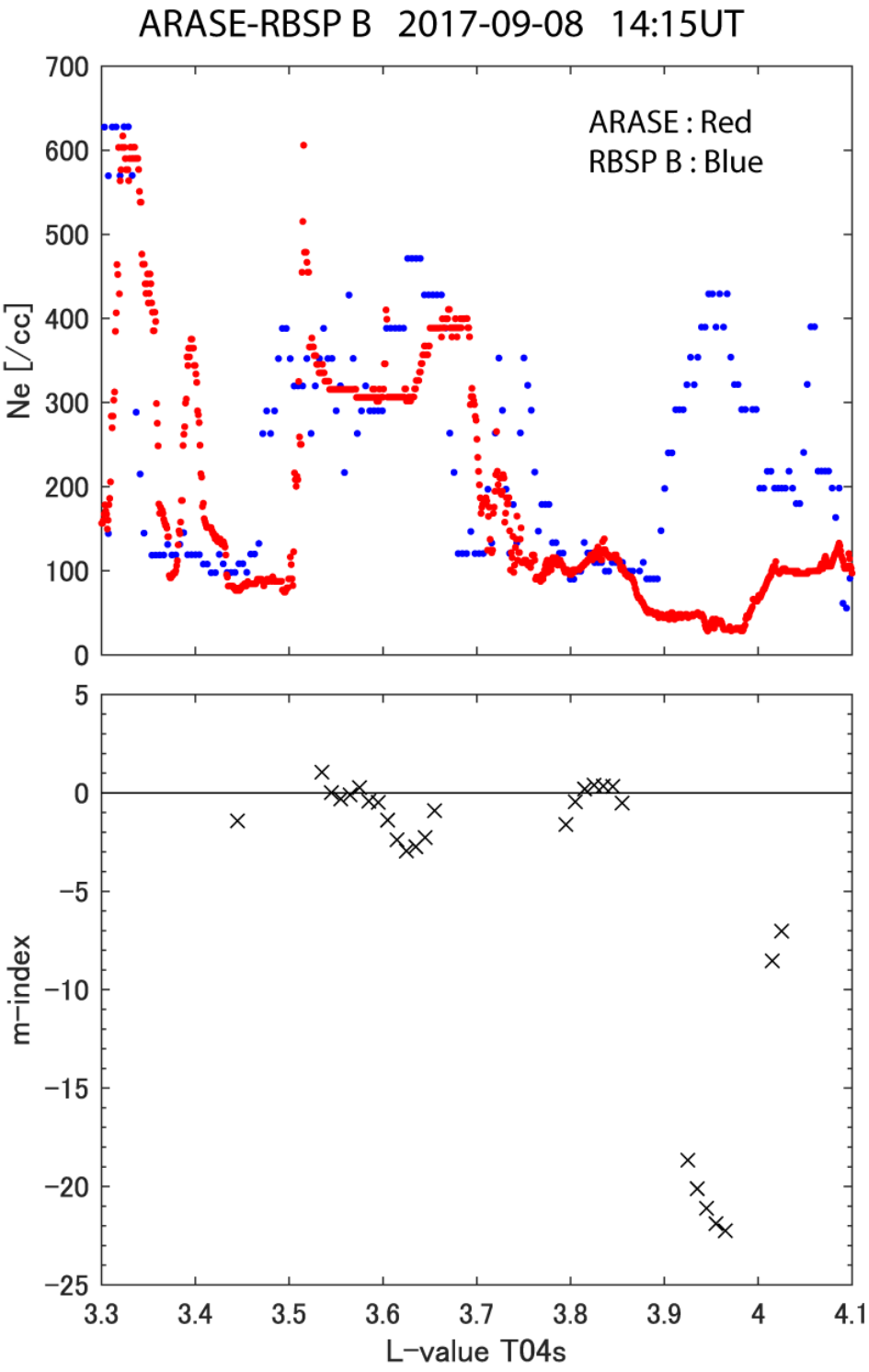
ARASE-RBSP B 2017-09-08 14:15UT
ARASE : Red
RBSP B : Blue
Ne [/cc]
m-index
L-value T04s

Figure 6

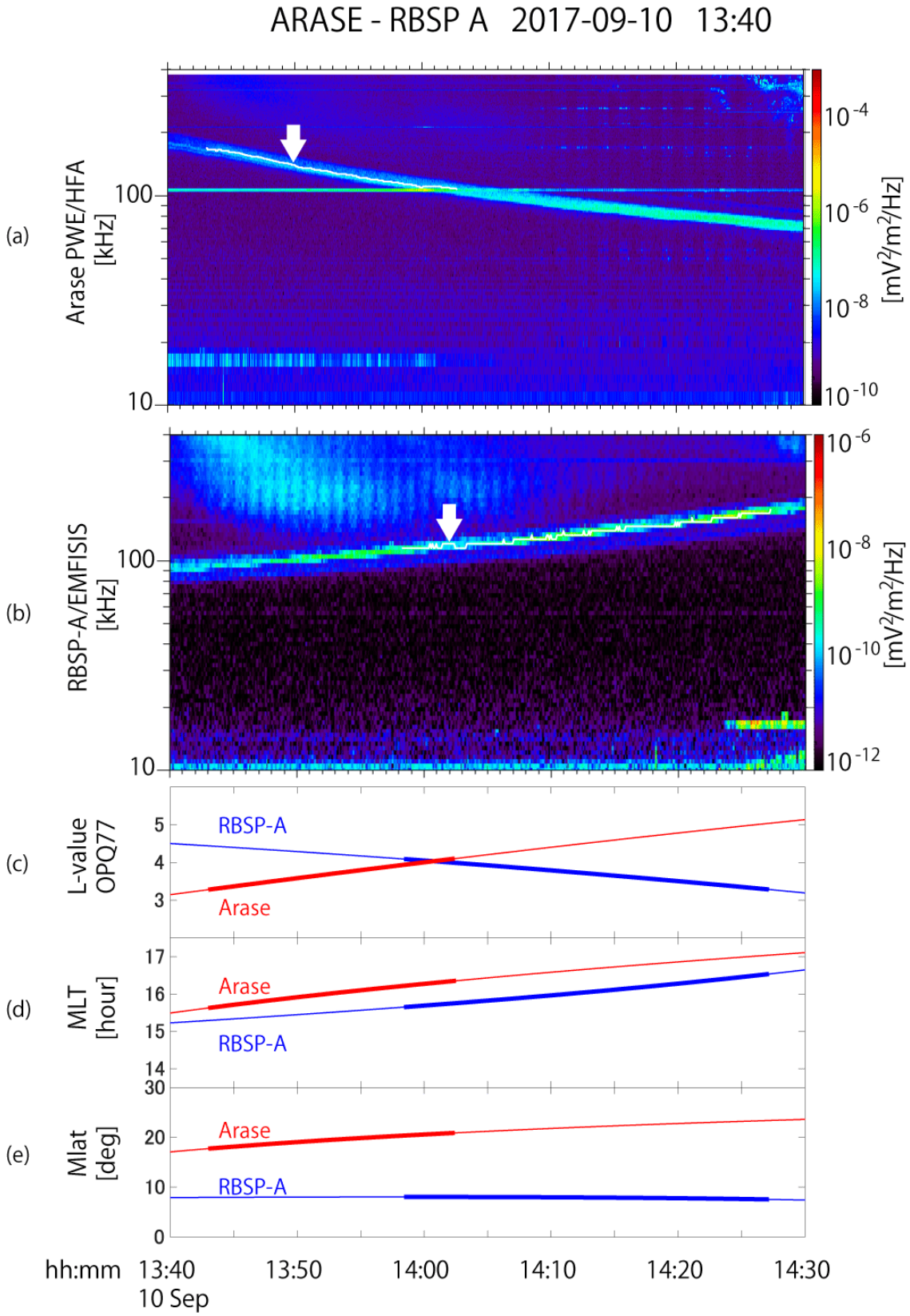

596

597 Figure 7

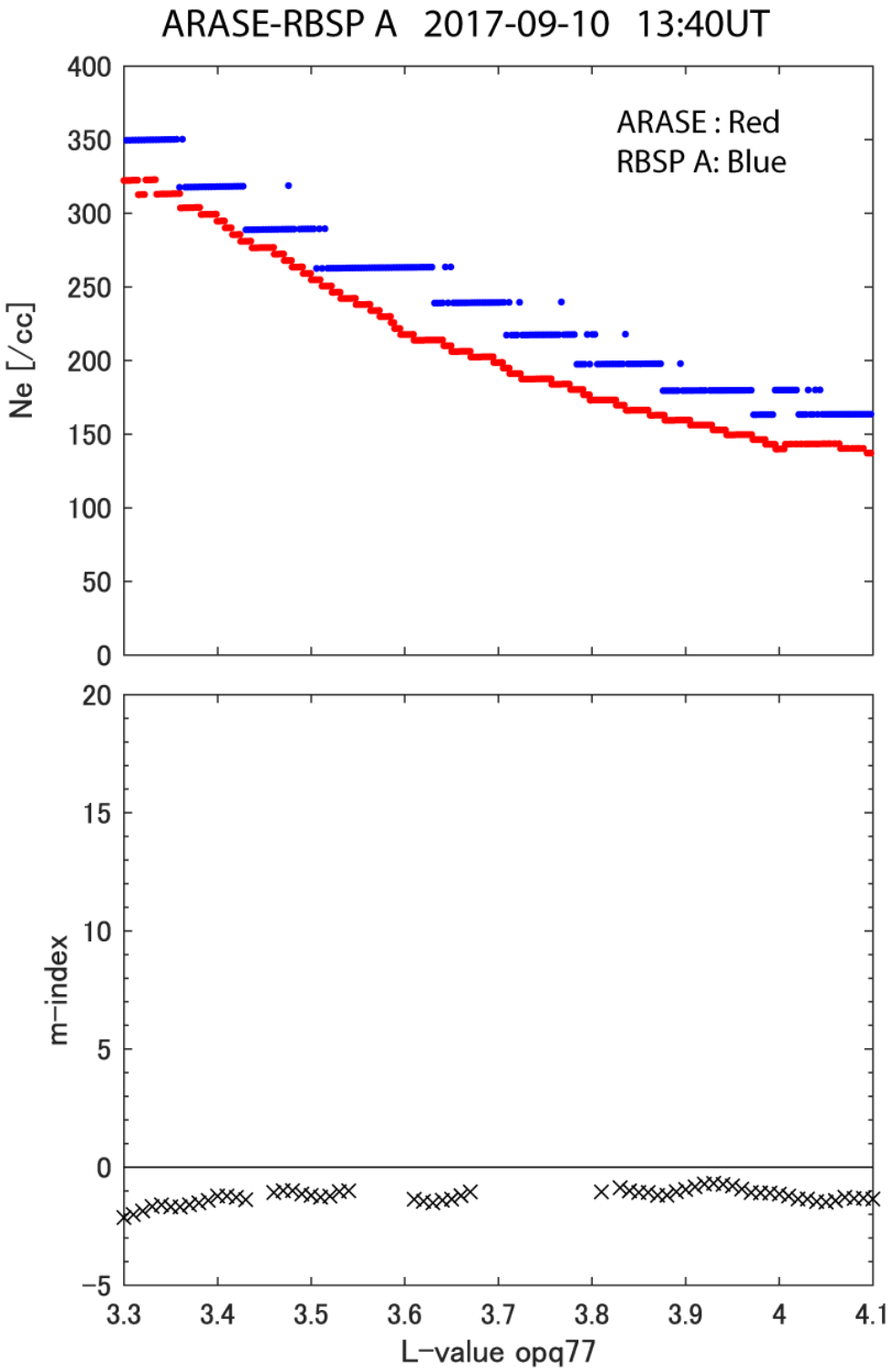

598

599

600 Figure 8